Geophys. J. Int. (2005) **160,** 89–100 doi: 10.1111/j.1365-246X.2005.02485.x

Apparent magnetic polarity reversals due to remagnetization resulting from late diagenetic growth of greigite from siderite

Leonardo Sagnotti,[1] Andrew P. Roberts,[2] Richard Weaver,[2] Kenneth L. Verosub,[3] Fabio Florindo,[1] Christopher R. Pike,[3] Trevor Clayton[2] and Gary S. Wilson[4]

[1] *Istituto Nazionale di Geofisica e Vulcanologia, Via di Vigna Murata,* 605, I-00143 *Rome, Italy. E-mail: sagnotti@ingv.it*
[2] *School of Ocean and Earth Science, University of Southampton, Southampton Oceanography Centre, European Way, Southampton* SO14 3ZH, *UK*
[3] *Department of Geology, University of California, Davis,* CA 95616, *USA*
[4] *Department of Geology, University of Otago, Dunedin, New Zealand*

Accepted 2004 October 1. Received 2004 September 8; in original form 2004 March 5

SUMMARY

A mixed-polarity zone, representing alternations between remagnetized and non-remagnetized strata, has been documented within the lower few metres of the CRP-1 core (Ross Sea, Antarctica). Detailed rock magnetic investigation of this interval indicates that the normal polarity remagnetization is carried by magnetostatically interacting single-domain particles of a ferrimagnetic iron sulphide mineral, while the reversed-polarity magnetization of non-remagnetized strata is carried by magnetite with a broad range of grain sizes and negligible magnetostatic interactions. Scanning electron microscope observations of polished sections indicate that the ferrimagnetic iron sulphide mineral is greigite (Fe_3S_4). Based on microtextural relationships, it is not possible to determine the relative timing of formation for much of the greigite. However, a significant proportion of the greigite has grown on the surface of authigenic siderite ($FeCO_3$) grains that occur as microconcretions and as cement surrounding detrital matrix grains. In such cases, microtextural relationships indicate that siderite post-dates early diagenetic pyrite and that greigite post-dates the siderite. Siderite usually forms in environments with abundant dissolved iron and carbonate, but without dissolved pore water H_2S. This set of geochemical conditions occurs in methanic settings below the sulphate reduction zone (in which early diagenetic pyrite forms). We interpret the observed remagnetization of the lower part of the CRP-1 core as due to a late diagenetic pore water migration event where abundant iron on the surface of siderite grains reacted with fluids containing limited dissolved sulphide, thereby causing precipitation of greigite. The distribution of siderite (and associated greigite) in the lower part of the CRP-1 core is patchy, which accounts for the apparent alternation of polarities. This study is part of a growing catalogue of remagnetizations involving greigite, which suggests that occurrences of greigite should be treated with caution in palaeomagnetic and environmental magnetic studies.

Key words: Antarctica, diagenesis, greigite, iron carbonate, iron sulphide, remagnetization, siderite.

1 INTRODUCTION

The reliability of a magnetic polarity stratigraphy depends on the validity of the assumption that the magnetic polarity recorded by a sedimentary sequence was acquired at or near the time of deposition. This assumption does not always hold, and it must be tested by carefully investigating the nature, origin and age of the magnetic minerals carrying the observed characteristic remanent magnetization (ChRM). There have recently been an increasing number of cases where the ferrimagnetic iron sulphide minerals greigite (Fe_3S_4) and pyrrhotite (Fe_7S_8) carry ChRMs with magnetic polarities opposite to those carried by coexisting magnetite or where the ChRM is contradictory to the expected polarity for the depositional age of the sedimentary sequence. These observations suggest a late, and sometimes complex, diagenetic origin for the iron sulphides (e.g. Florindo & Sagnotti 1995; Thompson & Cameron 1995; Horng *et al.* 1998; Richter *et al.* 1998; Xu *et al.* 1998; Dinarès-Turell & Dekkers 1999; Jiang *et al.* 2001; Weaver *et al.* 2002).

In this paper we report results from a detailed rock magnetic and scanning electron microscope (SEM) study of a mixed-polarity zone identified in the lowermost 4 m of the CRP-1 core from the Victoria Land Basin (Ross Sea, Antarctica), where an alternation of 18 magnetic polarity intervals was recognized (Roberts *et al.* 1998). The studied sediment is a homogeneous mudstone, which should

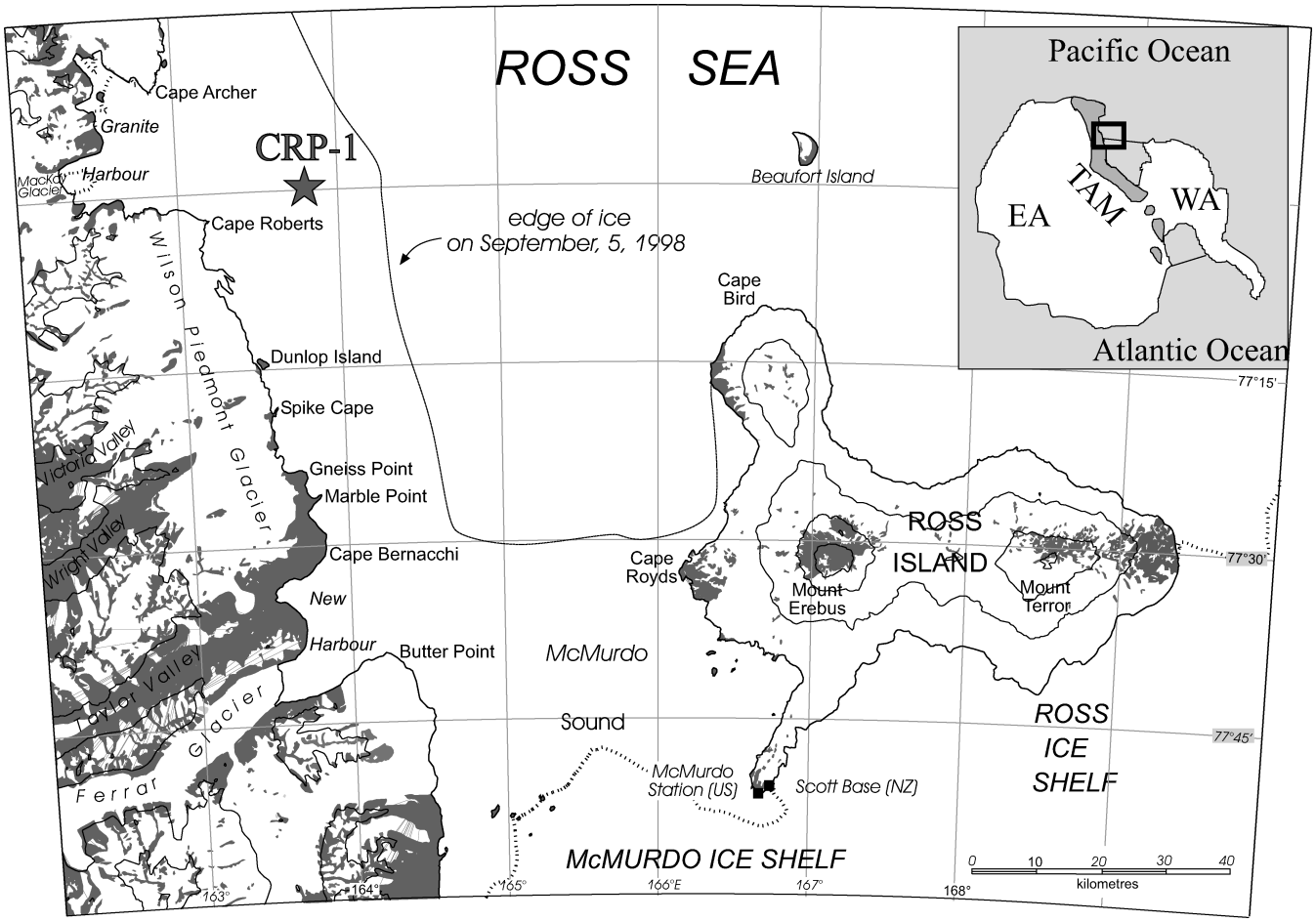

Figure 1. Location of the CRP-1 core, 16 km east of the Cape Roberts promontory. Palaeomagnetic measurements were made in a laboratory specially set up in McMurdo Station, Ross Island, for the Cape Roberts Project (Cape Roberts Project Science Team 1998; Roberts *et al.* 1998): EA, East Antarctica; WA, West Antarctica; TAM, Transantarctic Mountains.

be ideally suitable for magnetostratigraphic studies. Nevertheless, stratigraphic alternations in the magnetic mineralogy, which coincide with the observed polarity alternations, suggest that the polarity alternations do not represent a reliable recording of the ambient geomagnetic field during deposition (Roberts *et al.* 1998). In this paper, we document the mechanism that produced the observed remagnetization. This work emphasizes the danger of uncritically accepting the reliability of palaeomagnetic directions carried by authigenic magnetic iron sulphide minerals without detailed field tests and/or rock magnetic and petrographic investigations in support of palaeomagnetic studies.

2 GEOLOGICAL SETTING

The Cape Roberts Project was an international drilling programme aimed at investigating the early history of the East Antarctic ice sheet and the uplift of the Transantarctic Mountains by coring sedimentary strata at 77°S, at the edge of the present ice sheet. The CRP-1 core was drilled in October 1997 from a drill rig situated on a sea-ice platform, 16 km east-northeast of the Cape Roberts promontory in McMurdo Sound (Fig. 1). Drilling was terminated at 147.69 m below the seafloor (mbsf) because a major storm destroyed sea ice to within an unsafe distance of the drill rig. The recovered sediments include a Quaternary sequence between 16 and 43.55 mbsf and a lower Miocene sequence between 43.55 mbsf and the bottom of the hole at 147.69 mbsf (Cape Roberts Project Science Team 1998; Roberts *et al.* 1998). The core is divided into four Quaternary and three Miocene lithostratigraphic units, comprising 18 subunits (Cape Roberts Project Science Team 1998). Unit 7.1 is the deepest lithostratigraphic unit (Fig. 2) and consists of well-laminated siltstones and massive claystones. Contacts between the siltstones and the claystones are commonly sharp. Sandy-silty turbidites are also common in this unit and are characterized by inversely to normally graded well-laminated siltstones, with occasional dropstones (Howe *et al.* 1998). Unit 7.1 is interpreted to have been deposited in a quiet-water, ice-distal environment by settling of the fine fraction from suspension with little reworking by currents or gravity flows, and only episodic glacial influence (De Santis & Barrett 1998).

3 MAGNETOSTRATIGRAPHY

The original magnetostratigraphy of the CRP-1 core was based on measurements made on discrete samples during the drilling season in a palaeomagnetic laboratory specifically installed at McMurdo Station on Ross Island, Antarctica. Roberts *et al.* (1998) identified Unit 7.1 as a problematic 'mixed-polarity' zone. They recognized a clear delineation between a normal-polarity subvertical

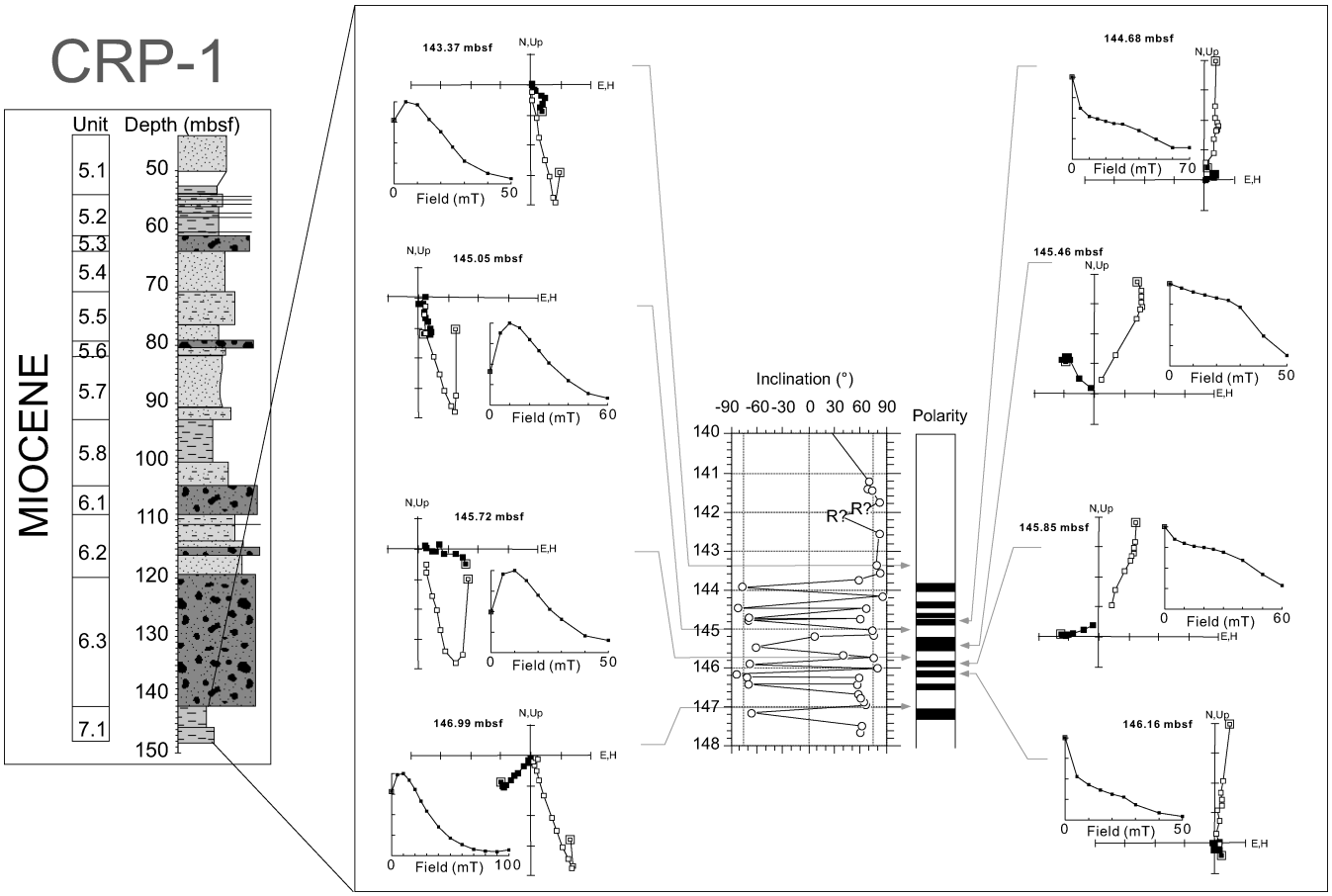

Figure 2. The original magnetostratigraphy of the CRP-1 core indicated the presence of a mixed-polarity zone in the lowermost 4 m of the CRP-1 core, with an alternation of 18 magnetic polarity intervals between 143.8 and 147.65 mbsf in Lithostratigraphic Unit 7.1 (Roberts *et al.* 1998). For reversed-polarity samples, the reversed-polarity characteristic remanent magnetization (ChRM) is distinct from a normal-polarity drilling-induced overprint. This distinction between the overprint and the ChRM is not as clear for many of the normal-polarity samples. NB: In the Southern Hemisphere, inclinations are negative (positive) for normal (reversed) polarity.

drilling-induced overprint and a reversed-polarity ChRM component for all of the reversed-polarity samples (Fig. 2), and concluded that the reversed-polarity data are reliable. However, clear delineation between the drilling-induced overprint and a 'characteristic' normal-polarity component is not always evident for the normal-polarity samples. If it is assumed that this mixed-polarity zone represents genuine geomagnetic field behaviour, then, based on independent constraints from diatom biostratigraphy (Harwood *et al.* 1998), maximum age constraints from $^{40}Ar/^{39}Ar$ dating of volcanic clasts in the sediments (McIntosh 1998) and $^{87}Sr/^{86}Sr$ dating of mollusc shells (Lavelle 1998), it could correlate with the 21–25 Myr interval of the geomagnetic polarity timescale (GPTS). With this interpretation, Unit 7.1 would represent a condensed section with a surprisingly low average sedimentation rate of about 1 m Myr^{-1} (Fig. 3). Such a low sedimentation rate is more characteristic of a sediment-starved environment and is highly unlikely in this glacimarine environment. Roberts *et al.* (1998) proposed a more plausible interpretation based on the observation that the observed high frequency of magnetic reversals coincides with marked alternations in basic magnetic properties of this part of the CRP-1 core, suggesting that the normal polarities might represent a remagnetization. However, the nature of the magnetic carriers in the normal-polarity intervals and the details of the magnetic mineralogy of the mixed-polarity zone were not fully identified in that study.

4 METHODS AND MEASUREMENTS

In this study, we present results of a more detailed rock magnetic investigation of the lower part of the CRP-1 core to assist in understanding the nature and origin of the mixed-polarity zone and coincident alternations in magnetic properties. Rock magnetic properties were measured using discrete cylindrical palaeomagnetic samples (25 mm diameter by 22 mm high) and powdered chip samples collected at an average spacing of 13 cm between 143.90 and 147.65 mbsf. Some measurements were made at McMurdo Station during the drilling season, but most were made afterwards at our home laboratories. Low-field magnetic susceptibility (κ) was measured on a Bartington Instruments MS2 magnetic susceptibility meter and on an AGICO KLY-2 Kappabridge magnetic susceptibility meter. Anhysteretic remanent magnetizations (ARMs) were produced in an alternating field (AF) of 100 mT, with a bias field of 0.1 mT. The ARM was imparted using a 2-G Enterprises cryogenic rock magnetometer system with an in-line AF demagnetizer and DC field solenoid. The ARM was then AF demagnetized in 10 mT steps up to 100 mT in order to determine the median destructive field (MDF_{ARM}). An isothermal remanent magnetization (IRM) was imparted in a succession of fields up to 1 T (IRM_{1T}). The IRM_{1T} was subsequently demagnetized in a series of back-fields up to −0.3 T in order to determine the coercivity of remanence (B_{cr}) and the *S* ratio

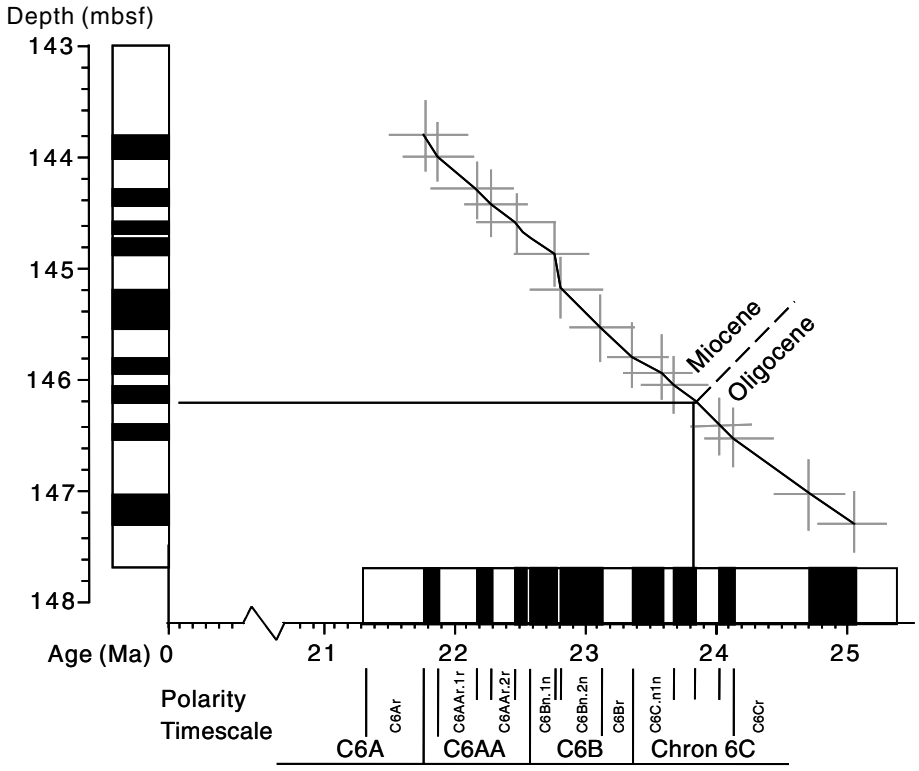

Figure 3. Possible one-to-one correlation of the observed magnetic polarities in Lithostratigraphic Unit 7.1 of the CRP-1 core to the geomagnetic polarity timescale (Cande & Kent 1995; Berggren *et al.* 1995) would lead to the estimate of a surprisingly low sedimentation rate of about 1 m Myr^{-1}. Such a rate is unrealistically low for a near-shore glacimarine environment.

($-\mathrm{IRM}_{-0.3\mathrm{T}}/\mathrm{IRM}_{1\mathrm{T}}$). The IRM was imparted using an ASC pulse magnetizer or a 2-G Enterprises pulse magnetizer and was measured using either an AGICO JR-5A spinner magnetometer or a 2-G Enterprises cryogenic magnetometer. Stepwise thermal demagnetization of a composite IRM (Lowrie 1990) was carried out by sequentially applying a pulsed magnetic field of 0.9, 0.5 and 0.12 T along the three orthogonal axes of representative samples. The composite IRM was thermally demagnetized at steps of 20, 120, 200, 250, 300, 350, 400, 450, 500, 550 and 600 °C. Hysteresis measurements were made on sediment chip samples using a Princeton Measurements Corporation MicroMag alternating gradient magnetometer. The standard hysteresis parameters were measured, including saturation magnetization (M_s), saturation remanent magnetization (M_r), coercive force (B_c) and coercivity of remanence (B_{cr}), as well as measurements of first-order reversal curves (FORCs), which were used to produce FORC diagrams (Pike *et al.* 1999; Roberts *et al.* 2000).

In addition to rock magnetic measurements, sediment microtextures were investigated for representative samples using polished thin sections in order to identify the diagenetic mineral phases responsible for the documented remagnetization. A LEO 1450VP SEM, operated at 15 keV at the Southampton Oceanography Centre, was used for these observations. Elemental analyses were obtained from energy-dispersive X-ray spectra (EDS) generated from point analyses (2–3 μm beam diameter) of individual mineral grains, or of clusters of grains, using a Princeton Gamma Tech (IMIX-PTS) system. The analyses were calibrated using a pyrite standard. EDS data yield iron to sulphur ratios that enable discrimination between the chemical formulae Fe_3S_4, FeS_2 and Fe_7S_8 for greigite, pyrite (Jiang *et al.* 2001) and pyrrhotite (Weaver *et al.* 2002), respectively. SEM analysis is therefore ideally suitable for discriminating between different iron sulphide species.

Table 1. Rock magnetic properties. See text for abbreviations and symbol definitions.

Parameters	Normal polarity, mean (S.D.)	Reverse polarity, mean (S.D.)
Concentration dependent		
κ (10×10^{-6} SI)	428.0 (48.6)	1240.3 (372.9)
NRM (A m^{-1})	8.92×10^{-3}	1.13×10^{-2}
	(5.80×10^{-3})	(1.21×10^{-2})
ARM (A m^{-1})	0.176 (0.048)	0.493 (0.085)
SIRM (A m^{-1})	7.0 (3.8)	18.6 (6.2)
M_r (A m^2)	2.01×10^{-2}	4.58×10^{-2}
	(1.05×10^{-2})	(1.58×10^{-2})
M_s (A m^2)	4.93×10^{-2}	1.72×10^{-1}
	(1.27×10^{-2})	(7.93×10^{-2})
Coercivity dependent		
S ratio	0.900 (0.036)	0.938 (0.029)
$\mathrm{MDF}_{\mathrm{ARM}}$ (mT)	42.5 (3.9)	28.5 (2.7)
B_c (mT)	30.1 (10.2)	18.0 (8.6)
B_{crpowder} (mT)	63.1 (10.3)	43.2 (11.1)
$B_{\mathrm{crcylinder}}$ (mT)	64.3 (4.6)	44.6 (9.3)
Interparametric ratios		
SIRM/κ (kA m^{-1})	17.2 (9.8)	14.8 (2.9)
M_r/M_s	0.39 (0.10)	0.29 (0.07)
B_{cr}/B_c	2.3 (0.8)	2.5 (0.4)

5 RESULTS

Mean values of rock magnetic parameters were calculated separately for the normal- and reversed-polarity samples (Table 1) and indicate a clear distinction between the two groups. Stratigraphic variations in the rock magnetic parameters indicate that they are closely related to the observed alternation of magnetic polarities

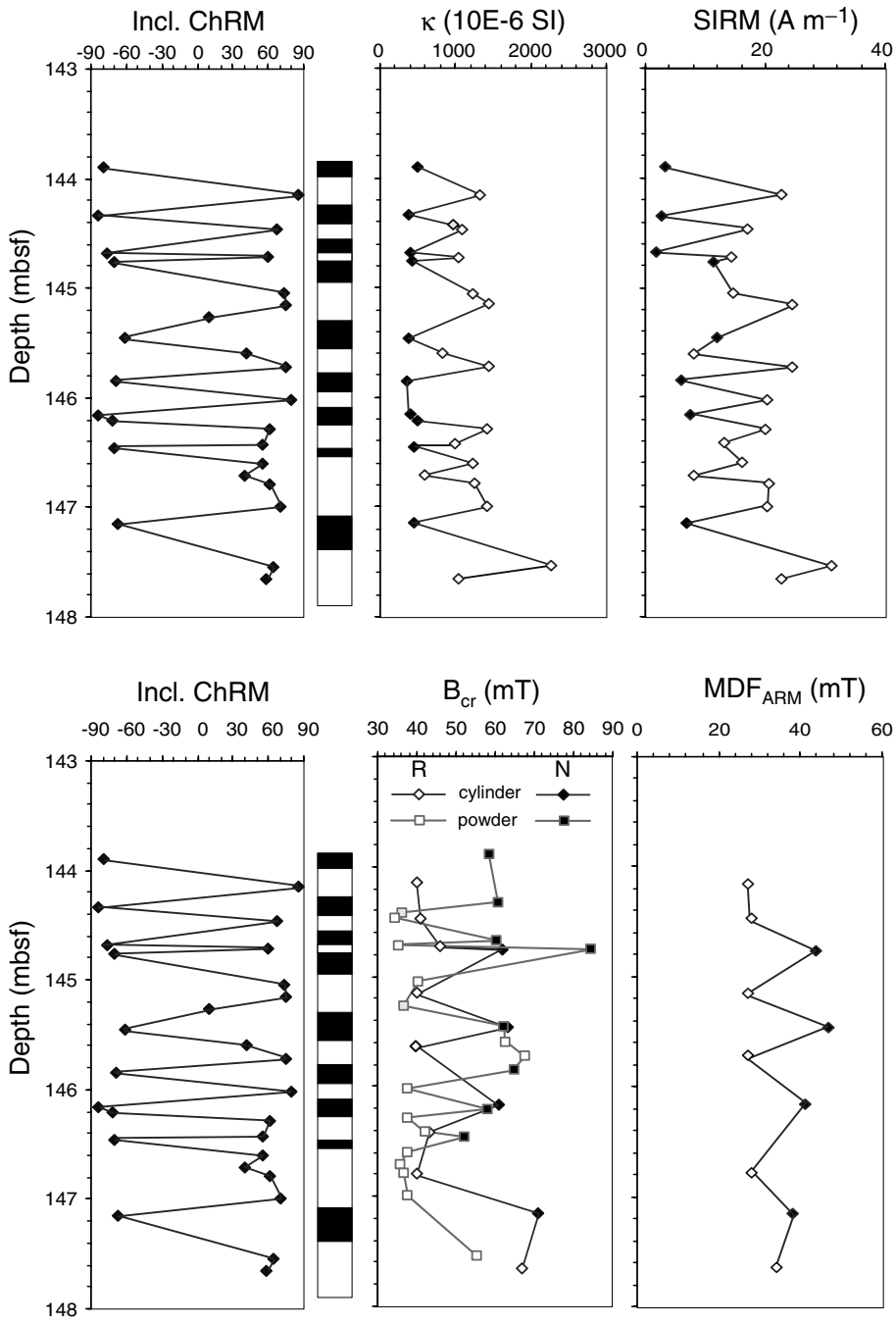

Figure 4. Down-core variation of the inclination of the ChRM and some selected rock magnetic parameters from the bottom of the CRP-1 core (κ, low-field magnetic susceptibility; SIRM, saturation isothermal remanent magnetization; B_{cr}, coercivity of remanence; MDF_{ARM}, median destructive field of the anhysteretic remanent magnetization). For the plots to the right of the magnetostratigraphic column, normal polarity is represented by full symbols and reversed polarity by open symbols. The results indicate coincident alternations of polarity and rock magnetic properties.

(Fig. 4). Reversed-polarity zones are generally characterized by relatively low coercivities (i.e. low B_{cr} and MDF_{ARM}), as well as by high values of rock magnetic parameters that mainly depend on the concentration of ferrimagnetic particles (i.e. high κ and saturation isothermal remanent magnetization (SIRM)). In contrast, normal-polarity zones are characterized by higher coercivities as well as by low values of the concentration-dependent parameters (Figs 4 and 5). The rock magnetic parameters of the normal- and reversed-polarity samples span non-overlapping ranges (Fig. 5), with a few exceptions for B_{cr} and SIRM.

All samples reached saturation of the IRM (SIRM) at the maximum applied field of 0.9 or 1 T. Thermal demagnetization of a composite IRM also reveals significant differences between the two groups of samples. The composite IRM of the reversed-polarity samples is dominated by the low-coercivity component, with a maximum unblocking temperature (T_{ub}) in the range between 550 and 600 °C (Fig. 6a), which indicates that magnetite is the main magnetic mineral in the reversed-polarity intervals. On the other hand, the data for the normal-polarity samples indicate that, in addition to magnetite (indicated by the predominance of the low-coercivity component

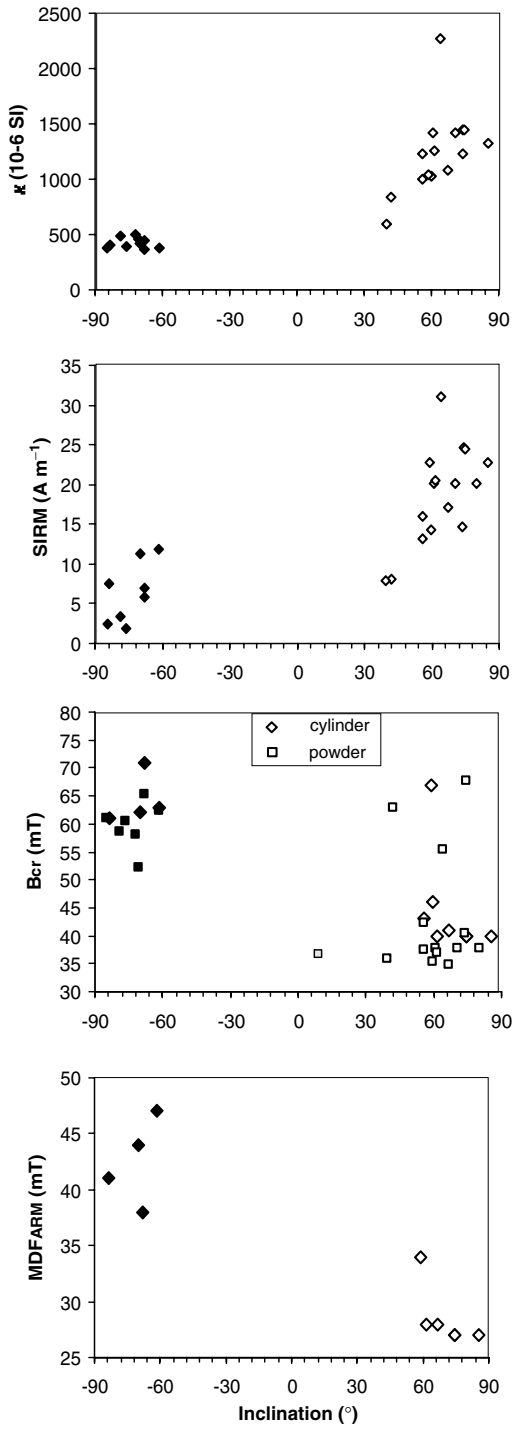

Figure 5. Selected rock magnetic parameters from the bottom of the CRP-1 core versus inclination of the ChRM. Normal polarity is represented by full symbols and reversed polarity by open symbols (magnetic parameters are the same as in Fig. 4). Normal-polarity samples are characterized by higher coercivities (i.e. higher B_{cr} and MDF_{ARM} values) and lower concentrations of magnetic minerals (i.e. lower κ and SIRM values) compared with the reversed-polarity samples.

and a maximum T_{ub} of 550–660 °C), there is also a significant contribution from a low- to intermediate-coercivity component with T_{ub} of 250–300 °C (Fig. 6b). This component is probably due to a ferrimagnetic iron sulphide mineral. Both pyrrhotite and greigite are characterized by moderate coercivities (IRM saturation is reached in fields <0.5 T and B_{cr} extends beyond the range typical for magnetite, up to 80–100 mT; Dekkers 1988; Roberts 1995; Dekkers & Schoonen 1996; Snowball 1997b). Both minerals also have a T_{ub} of ∼300 °C. Pyrrhotite has a Curie temperature in the range 300–350 °C (e.g. Dekkers 1988), while greigite thermally decomposes in air above 230 °C over a broad range of temperatures up to 380 °C (e.g. Roberts 1995; Sagnotti & Winkler 1999). Greigite is also well known to acquire significant spurious artificial magnetizations during AF treatment in fields higher than 40 mT (Snowball 1997a,b; Hu *et al.* 1998; Sagnotti & Winkler 1999) due to gyromagnetic effects (Stephenson 1980a,b) and similar behaviour during AF demagnetization has also been reported for pyrrhotite (Thomson 1990). Such gyromagnetic effects should produce noisy demagnetization data during tumbling AF demagnetization (Stephenson 1993). Despite the use of tumbling demagnetization in our palaeomagnetic study of this core (Roberts *et al.* 1998), we note that AF demagnetization data for samples from the studied interval are characterized by an apparently stable linear decrease toward the origin in fields up to 100 mT (Fig. 2).

Analysis of FORC diagrams confirms the clear distinction between the normal- and reversed-polarity samples and provides information about the domain state of the magnetic particles and the effects of magnetic interactions. The reversed-polarity intervals consist primarily of non-interacting single-domain and pseudo-single-domain grains with a superparamagnetic fraction and a coercivity distribution centred around 15 mT (Fig. 7a). The FORC distribution is consistent with a population of magnetite particles of variable grain size (Roberts *et al.* 2000). In contrast, the normal-polarity intervals consist primarily of interacting single-domain grains with a coercivity distribution centred around 50 mT (Fig. 7b). The presence of significant magnetostatic interactions and the observed range of coercivities are common for ferrimagnetic iron sulphide minerals (Roberts *et al.* 2000). The growth of greigite in framboidal clusters of crystals (e.g. Jiang *et al.* 2001) or the occurrence of pyrrhotite as intergrown crystals (e.g. Weaver *et al.* 2002) can explain why significant magnetic interactions are commonly observed for magnetic iron sulphides.

Rock magnetic analyses point clearly to the presence of magnetic iron sulphides in the remagnetized samples; however, they do not provide a clear discrimination between the possible presence of pyrrhotite as opposed to greigite. Backscattered electron imaging (BSEI) and EDS analyses using a SEM provide clear answers concerning the magnetic mineralogy. Pyrrhotite was not observed in any of the polished sections, either on the basis of expected Fe:S ratios or on the basis of its distinctive platy crystal habit (*cf.* Weaver *et al.* 2002). On the other hand, greigite is abundant in the analysed samples (Fig. 8). Polyframboidal iron sulphide aggregates are abundant (Fig. 8a), and consist of early diagenetic pyrite (FeS_2) framboids (circular cross-section with the brightest electron backscatter) that are surrounded by finer-grained (submicrometre) individual greigite octahedra that are usually less bright under BSEI (Figs 8a–d). Pyrite would be expected to have a lower electron backscatter than greigite because of its lower atomic weight; however, much of the observed greigite is very fine-grained with less regular surfaces that scatter electrons and produce a darker contrast than the smoother surfaces of coarser pyrite grains. The size of the iron sulphide aggregates is variable and ranges from a few micrometres to hundreds of micrometres across. These aggregates probably represent mineralized replacements of labile micro-organic matter, which provided a local microenvironment that was favourable for sulphidization reactions. This possibility is supported by the presence of a diatom fragment

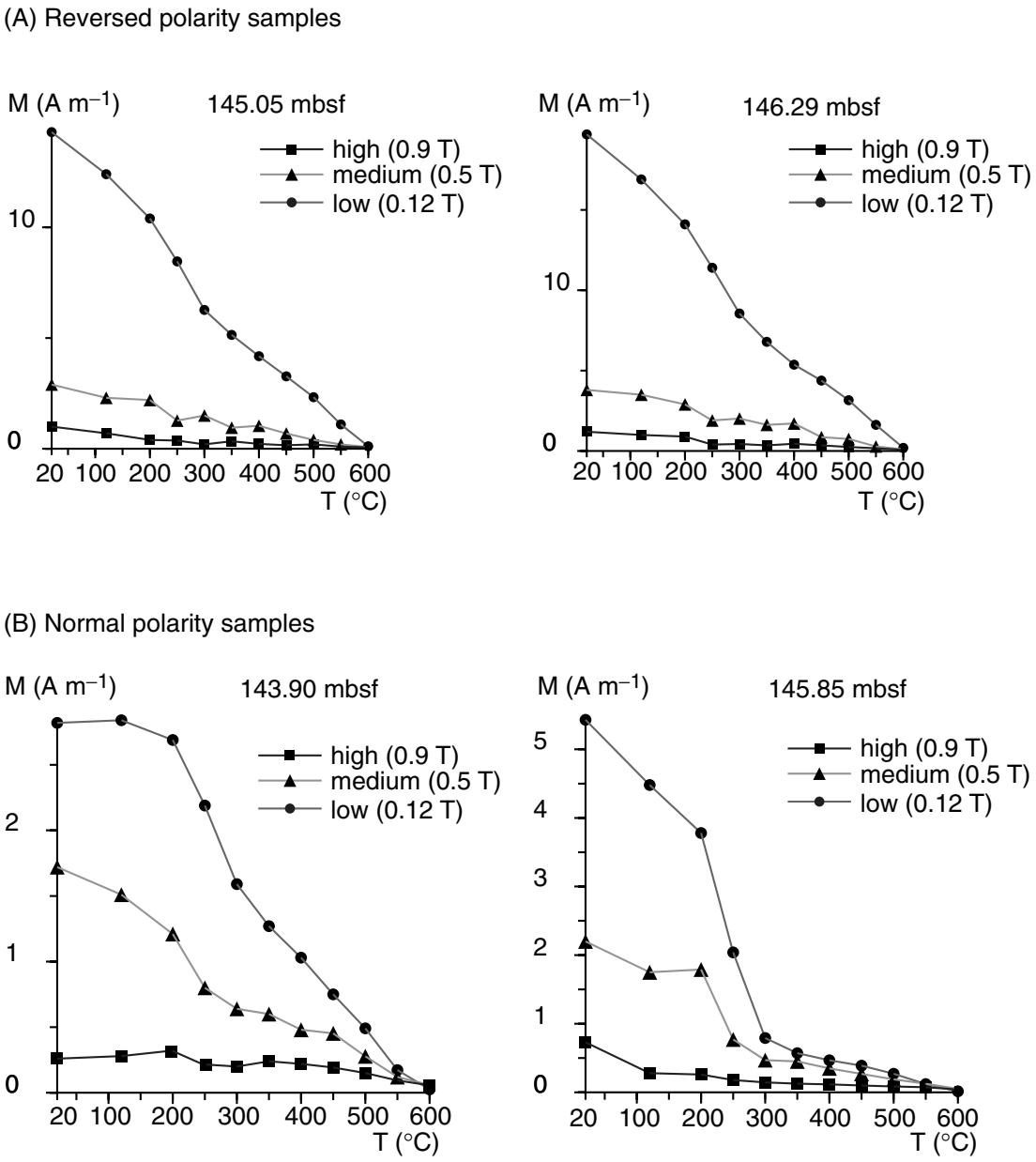

Figure 6. Representative thermal demagnetization data for a composite isothermal remanent magnetization produced in fields of 0.9, 0.5 and 0.12 T, respectively, along three mutually orthogonal sample axes: (a) reversed-polarity samples; (b) normal-polarity samples. See text for discussion.

remaining around the bottom edge of a mass of greigite particles, as shown in Fig. 8(d).

While it appears that the greigite has grown around earlier formed pyrite framboids (Figs 8a–d), these images do not provide conclusive evidence concerning the relative timing of greigite formation. In all of the remagnetized samples observed with the SEM, greigite is present in addition to the authigenic iron carbonate, siderite ($FeCO_3$). Microtextures of greigite associated with siderite provide much clearer evidence for the sequence of their authigenic growth compared with the polyframboidal aggregates that contain greigite. In a generalized view of the sediment matrix (Fig. 8e), framboidal pyrite is clearly present (circular cross-section with the brightest electron backscatter) in the interstices between detrital mineral grains. A carbonate (siderite) cement, which has similar electron backscatter to the surrounding detrital grains, has clearly grown around the early diagenetic pyrite framboids (Fig. 8e). This overgrowth is more clearly visible in a close-up image (Fig. 8f). In all cases where greigite occurs in association with siderite in the studied samples, the greigite has grown on the outer surfaces of the siderite (Fig. 8f). This indicates a progression in the growth of authigenic phases in the studied sediment, from pyrite to siderite to greigite. This observation has important implications for the remagnetization mechanism, which is discussed more fully below.

6 DISCUSSION AND CONCLUSIONS

The fine-scale structure of the observed magnetic polarity fluctuations in the basal part of the CRP-1 core is mirrored by fine-scale changes in magnetic mineralogy. Therefore, the alternation of polarities, as deduced from the ChRM directions, does not appear to represent a sequence of reversals of the geomagnetic field

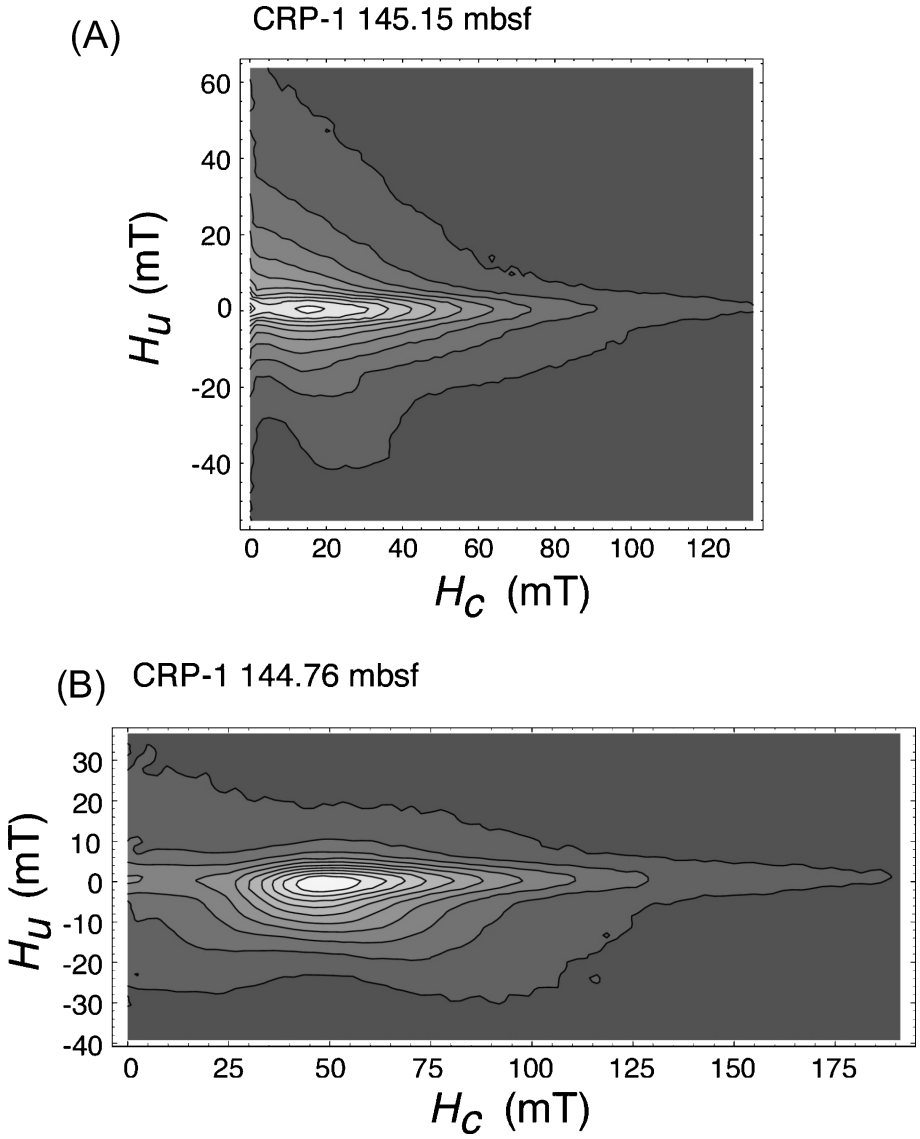

Figure 7. Representative FORC diagrams for samples from the bottom of the CRP-1 core: (a) reversed-polarity sample from 145.15 mbsf; (b) normal-polarity sample from 144.76 mbsf. By comparison with the interpretive framework of Roberts *et al.* (2000), these FORC diagrams are consistent with the presence of (a) negligibly magnetostatically interacting magnetite with a wide range of grain sizes (superparamagnetic, single domain, pseudo single domain) and (b) strongly magnetically interacting ferrimagnetic iron sulphide particles (greigite).

(Roberts *et al.* 1998). Instead, it reflects an alternation in composition and concentration of magnetic minerals at the scale of a few tens of centimetres. Reversed-polarity samples contain magnetite with variable grain size (in the pseudo-single-domain, single-domain and superparamagnetic-domain states). We infer that the reversed-polarity intervals in the CRP-1 core are likely to have faithfully recorded the polarity of the geomagnetic field at the time of deposition of Lithostratigraphic Unit 7.1. Normal-polarity samples are characterized by a more complex magnetic mineralogy, with strongly interacting single-domain particles of greigite and variable amounts of magnetite. The observed polarity alternations result from remagnetization of the normal-polarity intervals as a result of late diagenetic growth of greigite.

The nature of the authigenic mineral growth can be discussed in terms of two contrasting geochemical classifications, which can be used to explain our observations. Sedimentary microtextural evidence indicates a progression of diagenetic conditions that caused the successive authigenic growth of framboidal pyrite, followed by concretionary siderite and then growth of irregular patches of greigite octahedra (Fig. 8). Berner (1981) produced a geochemical classification of sedimentary environments that provides a framework for interpretation of the observed sequence of authigenic mineral growth. The presence of framboidal pyrite indicates that the studied sediments underwent sulphate reduction, where bacteria reduce sulphate from sea water to enable anaerobic decomposition of organic matter. Sulphate is reduced to H_2S or HS^-, which reacts with detrital iron-bearing minerals to form pyrite via intermediate phases such as mackinawite ($Fe_{1+x}S$) and greigite. If sufficient organic carbon is present, the natural diagenetic progression will result in consumption of all available pore-water sulphate by bacterial reduction so that methanogenesis occurs. Continued iron reduction at depth will result in a build-up of iron in the interstitial waters, which cannot react to form pyrite if H_2S is no longer being produced. The reduced iron will therefore be available to precipitate with other ions in solution. If the interstitial waters are saturated with respect to carbonate, siderite can form. Under this geochemical scenario, the formation

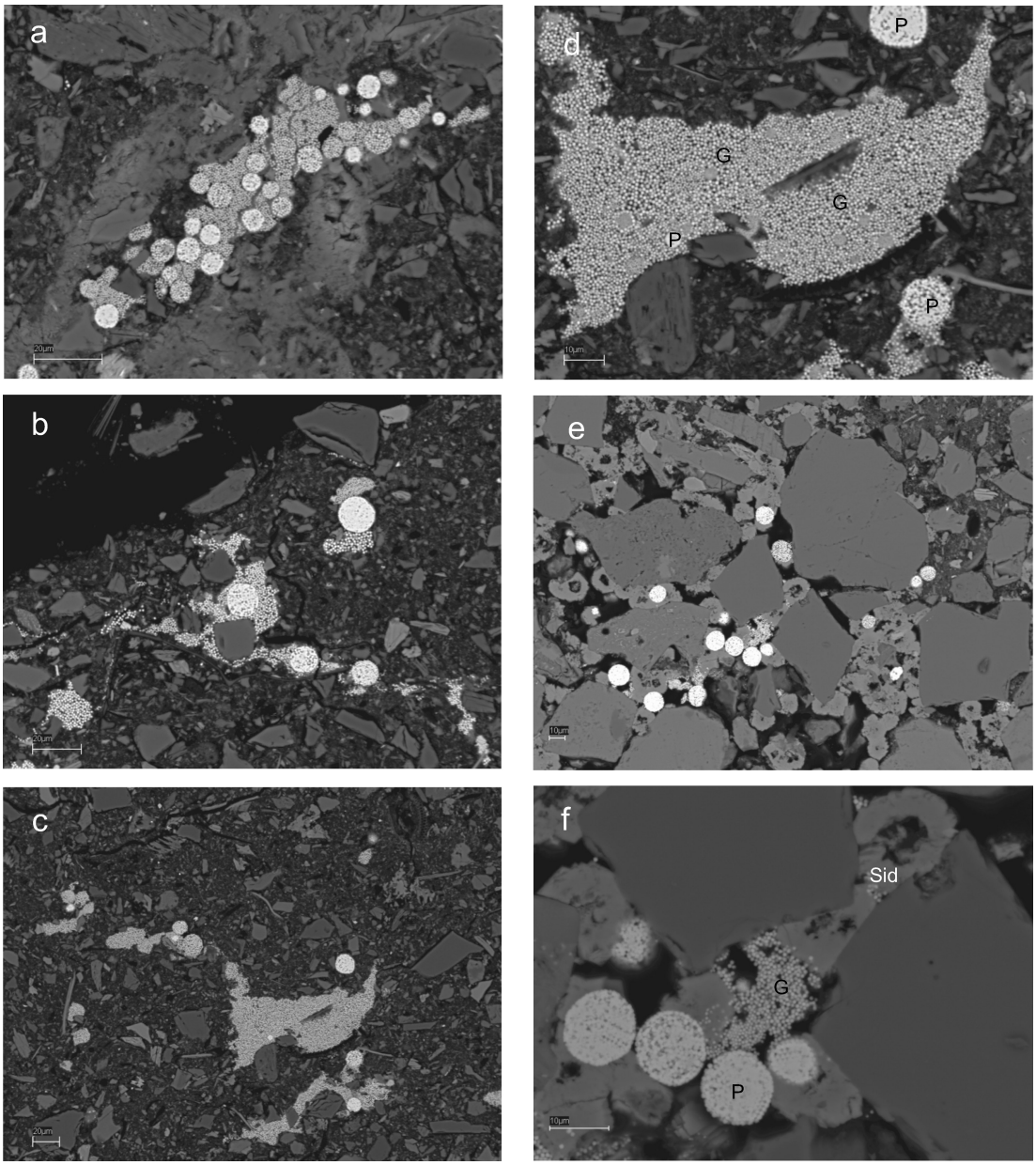

Figure 8. Representative backscattered electron photomicrographs for remagnetized samples from the lower part of the CRP-1 core. (a) Low-magnification view of a large polyframboidal aggregate of iron sulphide particles from 145.70 mbsf (scale bar = 20 μm). The large, bright aggregates with a round cross-section are pyrite framboids and the less bright, finer-grained individual octahedra are greigite particles. Microtextural relationships do not clearly indicate the timing of greigite growth except that it occurred after early diagenetic formation of the pyrite framboids. (b), (c) Other low-magnification views of polyframboidal aggregates of iron sulphide particles from 145.70 mbsf (scale bar = 20 μm). (d) Higher-magnification view of polyframboidal aggregates of iron sulphide particles from 145.70 mbsf: P, pyrite; G, greigite (scale bar = 10 μm). The presence of a diatom fragment at the bottom of the iron sulphide aggregate is consistent with formation of the iron sulphides as a result of organic matter remineralization. (e) View of the sediment matrix for a sample from 146.65 mbsf illustrating how siderite has filled and cemented the interstices between detrital grains (scale bar = 10 μm). The siderite has also clearly grown around the early diagenetic pyrite framboids (bright, with circular cross-section). (f) Close-up view of the interrelationship of siderite, pyrite and greigite for a sample from 146.65 mbsf: Sid, siderite (scale bar = 10 μm). The siderite has grown between detrital grains, and around pyrite framboids, but the greigite consistently appears on the surface of the siderite cement.

of greigite after siderite would require a later change in pore water chemistry. Siderite contains abundant reactive iron, and, if pore waters are sulphidic, it will react with dissolved sulphide to enable formation of iron sulphides. For example, laboratory synthesis of the iron sulphide mineral smythite (Fe_9S_{11}) makes use of the reactivity of iron in siderite to enable precipitation of smythite under sulphidic conditions (Rickard 1968; Furukawa & Barnes 1996). Sediments recovered in the CRP-1 core were never deeply buried (Baker & Fielding 1998) and changes in pore-water chemistry could have been induced by numerous mechanisms. For example, the chemistry of pore fluids will change in near-shore marine environments with variation in the position of the interface between fresh and saline ground water as a result of large-amplitude changes in relative sea level (e.g. Oda & Torii 2004) or as a result of glaciotectonically forced fluid migration due to over-riding of glaciers during ice advance events. As a modification of the scheme of Berner (1981),

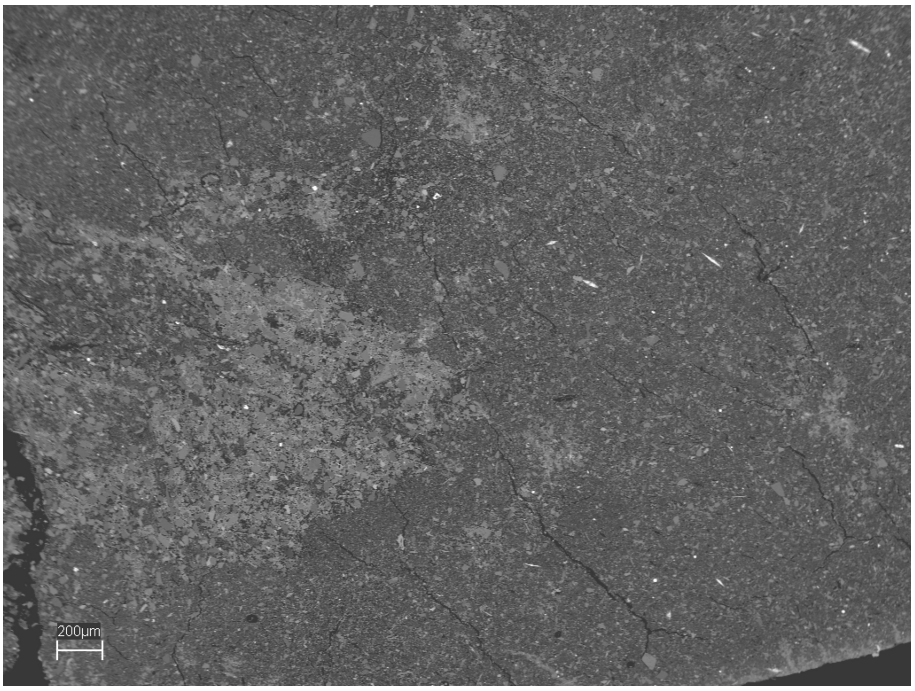

Figure 9. Representative low-magnification backscattered electron photomicrograph illustrating the patchy nature of the siderite cementation (slightly lighter electron backscatter on the left-hand side of the image) for a remagnetized sample from 144.68 mbsf (scale bar = 200 μm). As shown in Fig. 8(f), the remagnetization occurred when greigite grew authigenically on the surface of the siderite. The patchy nature of the siderite cementation is the most likely explanation for the apparent alternation of remagnetizations.

Raiswell (1997) argued that pore waters can contain small amounts of H_2S throughout the progression of diagenetic stages, and that small amounts of pyrite (and of its precursor, greigite) can form throughout diagenesis, including during methanogenesis. The presence of reactive iron on the surface of siderite grains and small residual amounts of pore water H_2S could therefore have given rise to greigite formation and the associated remagnetization without necessarily invoking a major change in pore-water chemistry.

In contrast to the diagenetic classification scheme of Berner (1981), Pye *et al.* (1990) showed that siderite and greigite can form simultaneously in sediments where the rate of iron reduction exceeds the rate of sulphate reduction. Lack of geochemical data for pore-water from the CRP-1 core precludes distinguishing between the formation of greigite via the hypothesized mechanisms of a localized change in pore-water chemistry or simultaneous growth with siderite. However, we favour the first mechanism because the greigite occurs on the surfaces of siderite grains and therefore appears to have grown after the siderite. Siderite has formed in many intervals within the CRP-1 core (Baker & Fielding 1998; Claps & Aghib 1998), but the lowermost part of the CRP-1 core is the only interval in which we have identified authigenic greigite, let alone a remagnetization carried by greigite. This observation also favours our interpretation that pore-water conditions were different in the lower parts of the core compared with the upper parts.

While there have been previous reports of the co-occurrence of greigite and siderite, they mainly involve studies of active depositional/diagenetic environments (e.g. Postma 1977; Pye 1981; Pye *et al.* 1990) and reports of co-preservation of these phases in the geological record are sparse (exceptions include Krs *et al.* 1992; Krupp 1994). Additional reports of co-occurrences of siderite and magnetic iron sulphides in the geological record involve smythite or pyrrhotite (see Erd *et al.* 1957—but see subsequent redefinition of smythite by Taylor & Williams (1972) and see also Novák & Jansa (1992), Hoffmann *et al.* (1993) and Furukawa & Barnes (1996) and references therein). Thus, while the co-occurrence of siderite and magnetic iron sulphides has been previously documented, our results demonstrate for the first time a remagnetization involving a combined occurrence of greigite and siderite. Despite the fact that a clear link has not previously been made between the co-occurrence of greigite and siderite and a remagnetization carried by late diagenetic greigite, this observation is not surprising. Several studies have documented remagnetizations involving authigenic iron sulphide minerals that formed as a result of reactions between sulphidic pore fluids and either authigenic or detrital iron-bearing phases (e.g. Florindo & Sagnotti 1995; Richter *et al.* 1998; Dinarès-Turell & Dekkers 1999; Jiang *et al.* 2001; Weaver *et al.* 2002). The growing catalogue of locations where greigite has been implicated in late diagenetic remagnetizations suggests that its identification should lead to caution in interpretation of palaeomagnetic and environmental magnetic data.

The distribution of siderite in the lower part of the CRP-1 core is patchy (e.g. Fig. 9), which is a common mode of growth for siderite cements (e.g. Raiswell & Fisher 2000). The patchy nature of the siderite cementation (and the greigite associated with it) explains the apparent alternation of polarities.

Siderite (and other iron-bearing carbonates) has an inverse magnetic fabric (Rochette 1988; Ihmlé *et al.* 1989; Rochette *et al.* 1992; Winkler *et al.* 1996), where the minimum susceptibility axis ($k_{\min}$) of the AMS ellipsoid lies within the bedding plane. Single-domain ferrimagnetic particles are also known to give rise to inverse AMS fabrics (Potter & Stephenson 1988). Therefore, greigite particles, which typically have single-domain-like magnetic properties (Roberts 1995; Sagnotti & Winkler 1999), should theoretically also produce an inverse AMS fabric. However, both the normal- and reversed-polarity samples from Lithostratigraphic Unit 7.1 of the CRP-1 core have normal AMS fabrics, with subvertical $k_{\min}$ axes

(i.e. perpendicular to the bedding plane) and oblate AMS ellipsoids (see Fig. 6 in Sagnotti *et al.* 1998). The only sample with a prolate AMS ellipsoid and a 30° inclination of the k_{min} axes is from a reversed-polarity sample from the bottom of the core (147.65 mbsf) with negligible greigite and siderite content. We attribute the anomalous AMS of this sample to drilling-induced deformation at the bottom of the drill-hole. The AMS data of Sagnotti *et al.* (1998), coupled with the detailed magnetic mineralogical observations reported in this study, lead to two conclusions: (1) the content of siderite in the CRP-1 samples is insufficient to have overcome the contribution to the overall magnetic susceptibility of all other grains with normal AMS fabric (i.e. the paramagnetic clay matrix and ferrimagnetic mineral grains) and (2) aggregates of single-domain-like greigite contradict theoretical predictions that such material should produce an inverse AMS fabric. The lack of inverse and intermediate AMS fabrics in samples where greigite dominates the magnetic behaviour has already been pointed out by Sagnotti & Winkler (1999) for fine-grained sediments throughout Italy and has been subsequently verified in other geological contexts (Aubourg & Robion 2002). At present, there is no theoretical explanation for this observation.

Finally, siderite is paramagnetic at room temperature (Jacobs 1963). Its presence in a sediment would therefore not normally be considered to be palaeomagnetically important. However, siderite is unstable in oxic weathering environments, where it can transform into iron oxides that can carry a stable secondary magnetization (Ellwood *et al.* 1986). Pan *et al.* (2000) also showed that care should be taken when thermally demagnetizing rocks containing siderite because similar oxidative mineralogical transformations occur during heating. We have demonstrated that alteration of siderite can also cause remagnetization in reducing environments, which extends the previously known range of environments in which the presence of siderite can compromise a palaeomagnetic record. Thus, as is the case with greigite, identification of siderite should also lead to caution when interpreting palaeomagnetic and environmental magnetic data. Developments in the use of low-temperature magnetic properties (Housen *et al.* 1996; Frederichs *et al.* 2003) usefully augment the standard mineralogical methods for identifying siderite and for taking into account its effects on the magnetic signature of the rocks in which it occurs.

ACKNOWLEDGMENTS

The Cape Roberts Project was a multinational effort and drilling was made possible by the resources and close collaboration of the Antarctic programmes of Australia, Germany, Italy, New Zealand, the United Kingdom and the United States of America, with field operations organized by Antarctica New Zealand. The authors also acknowledge the support of their home institutions and funding agencies. We are grateful to Richard Pearce (Southampton Oceanography Centre) for assistance with setting up the SEM for quantitative microanalysis. Reviews by Tilo von Dobeneck and an anonymous referee helped to improve the manuscript.

REFERENCES

Aubourg, C. & Robion, P., 2002. Composite ferromagnetic fabrics (magnetite, greigite) measured by AMS and partial AARM in weakly strained sandstones from western Makran, Iran, *Geophys. J. Int.,* **151,** 729–737.

Baker, J.C. & Fielding, C.R., 1998. Diagenesis of glacimarine Miocene strata in CRP-1, Antarctica, *Terra Antartica,* **5,** 647–653.

Berggren, W.A., Kent, D.V., Swisher, C.C., III & Aubry, M.P., 1995. A revised Cenozoic geochronology and biostratigraphy, in *Geochronology, Time Scales, and Stratigraphic Correlation,* SEPM Special Publication 54, pp. 129–212, eds Berggren, W.A., Kent, D.V., Aubry, M.P. & Hardenbol, J., Society of Economic Paleontologists and Mineralogists, Tulsa, OK.

Berner, R.A., 1981. A new geochemical classification of sedimentary environments, *J. Sediment. Petrol.,* **51,** 359–365.

Cande, S.C. & Kent, D.V., 1995. Revised calibration of the geomagnetic polarity timescale for the Late Cretaceous and Cenozoic, *J. geophys. Res.,* **100,** 6093–6095.

Cape Roberts Project Science Team, 1998. Initial report on CRP-1, Cape Roberts Project, Antarctica, *Terra Antartica,* **5,** 1–187.

Claps, M. & Aghib, F.S., 1998. Carbonate diagenesis in Miocene sediments from CRP-1, Victoria Land Basin, Antarctica, *Terra Antartica,* **5,** 655–660.

Dekkers, M.J., 1988. Magnetic properties of natural pyrrhotite part I: behaviour of initial susceptibility and saturation-magnetisation-related rock-magnetic parameters in a grain-size dependent framework, *Phys. Earth planet. Inter.,* **52,** 376–394.

Dekkers, M.J. & Schoonen, M.A.A., 1996. Magnetic properties of hydrothermally synthesized greigite (Fe_3S_4)—I. Rock magnetic parameters at room temperature, *Geophys. J. Int.,* **126,** 360–368.

De Santis, L. & Barrett, P.J., 1998. Grain size analysis of samples from CRP-1, *Terra Antartica,* **5,** 375–382.

Dinarès-Turell, J. & Dekkers, M.J., 1999. Diagenesis and remanence acquisition in the Lower Pliocene Trubi marls at Punta di Maiata (southern Sicily): palaeomagnetic and rock magnetic observations, in *Palaeomagnetism and Diagenesis in Sediments,* Geological Society of London Special Publication 151, pp. 53–69, eds Tarling, D.H. & Turner, P., Geological Society of London, London.

Ellwood, B.B., Balsam, W., Burkart, B., Long, G.J. & Buhl, M.L., 1986. Anomalous magnetic properties in rocks containing the mineral siderite: paleomagnetic implications, *J. geophys. Res.,* **91,** 12 779–12 790.

Erd, R.C., Evans, H.T. Jr, & Richter, D.H., 1957. Smythite, a new iron sulfide, and associated pyrrhotite from Indiana, *Am. Mineral.,* **42,** 309–333.

Florindo, F. & Sagnotti, L., 1995. Palaeomagnetism and rock magnetism in the upper Pliocene Valle Ricca (Rome, Italy) section, *Geophys. J. Int.,* **123,** 340–354.

Frederichs, T., von Dobeneck, T., Bleil, U. & Dekkers, M.J., 2003. Towards the identification of siderite, rhodochrosite, and vivianite in sediments by their low-temperature magnetic properties, *Phys. Chem. Earth,* **28,** 669–679.

Furukawa, Y. & Barnes, H.L., 1996. Reactions forming smythite, Fe_9S_{11}, *Geochim. Cosmochim. Acta,* **60,** 3581–3591.

Harwood, D.M., Bohaty, S.M. & Scherer, R.P., 1998. Lower Miocene diatom biostratigraphy of the CRP-1 drillcore, McMurdo Sound, Antarctica, *Terra Antarctica,* **5,** 499–514.

Hoffmann, V., Stanjek, H. & Murad, E., 1993. Mineralogical, magnetic and Mössbauer data of smythite (Fe_9S_{11}), *Stud. Geophys. Geodaet.,* **37,** 366–381.

Horng, C.-S., Torii, M., Shea, K.-S. & Kao, S.-J., 1998. Inconsistent magnetic polarities between greigite- and pyrrhotite/magnetite-bearing marine sediments from the Tsailiao-chi section, southwestern Taiwan, *Earth planet. Sci. Lett.,* **164,** 467–481.

Housen, B.A., Banerjee, S.K. & Moskowitz, B.M., 1996. Low-temperature magnetic properties of siderite and magnetite in marine sediments, *Geophys. Res. Lett.,* **23,** 2843–2846.

Howe, J.A., Woolfe, K.J. & Fielding, C.R., 1998. Lower Miocene glacimarine gravity flows, Cape Roberts Drillhole-1, Ross Sea, Antarctica, *Terra Antartica,* **5,** 393–399.

Hu, S., Appel, E., Hoffmann, V., Schmahl, W.W. & Wang, S., 1998. Gyromagnetic remanence acquired by greigite (Fe_3S_4) during static three-axis alternating field demagnetization, *Geophys. J. Int.,* **134,** 831–842.

Ihmlé, P.F., Hirt, A.M. & Lowrie, W., 1989. Inverse magnetic fabric in deformed limestones of the Morcles nappe, Switzerland, *Geophys. Res. Lett.,* **16,** 1383–1386.

Jacobs, I.S., 1963. Metamagnetism of siderite ($FeCO_3$), *J. Appl. Phys.,* **34,** 1106–1107.

Jiang, W.T., Horng, C.S., Roberts, A.P. & Peacor, D.R., 2001. Contradictory magnetic polarities in sediments and variable timing of neoformation of authigenic greigite, *Earth planet. Sci. Lett.,* **193,** 1–12.

Krs, M., Novák, F., Krsová, M., Pruner, P., Kouklíková, L. & Jansa, J., 1992. Magnetic properties and metastability of greigite-smythite mineralization in brown-coal basins of the Krusné Hory Piedmont, Bohemia, *Phys. Earth planet. Inter.,* **70,** 273–287.

Krupp, R.E., 1994. Phase relations and phase transformations between the low-temperature iron sulphides mackinawite, greigite, and smythite, *Eur. J. Mineral.,* **6,** 265–278.

Lavelle, M., 1998. Strontium-isotope stratigraphy of the CRP-1 drillhole, Ross Sea, Antarctica, *Terra Antartica,* **5,** 691–696.

Lowrie, W., 1990. Identification of ferromagnetic minerals in a rock by coercivity and unblocking temperature properties, *Geophys. Res. Lett.,* **17,** 159–162.

McIntosh, W.C., 1998. $^{40}Ar/^{39}Ar$ geochronology of volcanic clasts and pumice in CRP-1 core, Cape Roberts, Antarctica, *Terra Antartica,* **5,** 683–690.

Novák, F. & Jansa, J., 1992. Authigenic smythite and pyrrhotite in the upper part of the Sokolov Formation (the Sokolov Basin, Czechoslovakia), *Bull. Geol. Surv. Prague,* **67,** 235–244.

Oda, H. & Torii, M., 2004. Sea-level change and remagnetization of continental shelf sediments off New Jersey (ODP Leg 174A): magnetite and greigite diagenesis, *Geophys. J. Int.,* **156,** 443–458.

Pan, Y., Zhu, R. & Banerjee, S.K., 2000. Rock magnetic properties related to thermal treatment of siderite: behavior and interpretation, *J. geophys. Res.,* **105,** 783–794.

Pike, C.R., Roberts, A.P. & Verosub, K.L., 1999. Characterizing interactions in fine magnetic particle systems using first order reversal curves, *J. Appl. Phys.,* **85,** 6660–6667.

Postma, D., 1977. The occurrence and chemical composition of recent Fe-rich mixed carbonates in a river bog, *J. Sediment. Petrol.,* **47,** 1089–1098.

Potter, D.K. & Stephenson, A., 1988. Single-domain particles in rocks and magnetic fabric analysis, *Geophys. Res. Lett.,* **15,** 1097–1100.

Pye, K., 1981. Marshrock formed by iron sulphide and siderite cementation in saltmarsh sediments, *Nature,* **294,** 650–652.

Pye, K., Dickson, J.A.D., Schiavon, N., Coleman, M.L. & Cox, M., 1990. Formation of siderite-Mg-calcite-iron sulphide concretions in intertidal marsh and sandflat sediments, north Norfolk, England, *Sedimentology,* **37,** 325–343.

Raiswell, R., 1997. A geochemical framework for the application of stable sulphur isotopes to fossil pyritization, *J. geol. Soc. Lond.,* **154,** 343–356.

Raiswell, R. & Fisher, Q.J., 2000. Mudrock-hosted carbonate concretions: a review of growth mechanisms and their influence on chemical and isotopic composition, *J. geol. Soc. Lond.,* **157,** 239–251.

Richter, C., Roberts, A.P., Stoner, J.S., Benning, L.D. & Chi, C.T., 1998. Magnetostratigraphy of Pliocene–Pleistocene sediments from the eastern Mediterranean Sea, *Proc. ODP, Sci. Res.,* **160,** 61–74.

Rickard, D.T., 1968. Synthesis of smythite-rhombohedral Fe_3S_4, *Nature,* **218,** 356–357.

Roberts, A.P., 1995. Magnetic properties of sedimentary greigite (Fe_3S_4), *Earth planet. Sci. Lett.,* **134,** 227–236.

Roberts, A.P., Wilson, G.S., Florindo, F., Sagnotti, L., Verosub, K.L. & Harwood, D.M., 1998. Magnetostratigraphy of lower Miocene strata from the CRP-1 core, McMurdo Sound, Ross Sea, Antarctica, *Terra Antartica,* **5,** 703–713.

Roberts, A.P., Pike, C.R. & Verosub, K.L., 2000. FORC diagrams: a new tool for characterizing the magnetic properties of natural samples, *J. geophys. Res.,* **105,** 28 461–28 475.

Rochette, P., 1988. Inverse magnetic fabric in carbonate-bearing rocks, *Earth planet. Sci. Lett.,* **90,** 229–237.

Rochette, P., Jackson, M. & Aubourg, C., 1992. Rock magnetism and the interpretation of anisotropy of magnetic susceptibility, *Rev. Geophys.,* **30,** 209–226.

Sagnotti, L. & Winkler, A., 1999. Rock magnetism and palaeomagnetism of greigite-bearing mudstones in the Italian peninsula, *Earth planet. Sci. Lett.,* **165,** 67–80.

Sagnotti, L., Florindo, F., Wilson, G.S., Roberts, A.P. & Verosub, K.L., 1998. Environmental magnetism of lower Miocene strata from the CRP-1 core, McMurdo Sound, Antarctica, *Terra Antartica,* **5,** 661–667.

Snowball, I.F., 1997a. Gyroremanent magnetization (GRM) and the magnetic properties of greigite bearing clays in southern Sweden, *Geophys. J. Int.,* **129,** 624–636.

Snowball, I.F., 1997b. The detection of single-domain greigite (Fe_3S_4) using rotational remanent magnetization (RRM) and the effective gyro field (B_g): mineral magnetic and palaeomagnetic applications, *Geophys. J. Int.,* **130,** 704–716.

Stephenson, A., 1980a. Gyromagnetism and the remanence acquired by a rotating rock in an alternating field, *Nature,* **284,** 48–49.

Stephenson, A., 1980b. A gyroremanent magnetization in anisotropic magnetic material, *Nature,* **284,** 49–51.

Stephenson, A., 1993. Three-axis static alternating-field demagnetization of rocks and the identification of NRM, GRM, and anisotropy, *J. geophys. Res.,* **98,** 373–381.

Taylor, L.A. & Williams, K.L., 1972. Smythite $(Fe, Ni)_9S_{11}$—a redefinition, *Am. Mineral.,* **57,** 1571–1577.

Thompson, R. & Cameron, T.J.D., 1995. Palaeomagnetic study of Cenozoic sediments in North Sea boreholes: an example of a magnetostratigraphic conundrum in a hydrocarbon-producing area, in *Palaeomagnetic Applications in Hydrocarbon Exploration,* Geological Society of London Special Publication 98, pp. 223–236, eds Turner, P. & Turner, A., Geological Society of London, London.

Thomson, G.F., 1990. The anomalous demagnetisation of pyrrhotite, *Geophys. J. Int.,* **103,** 425–430.

Weaver, R., Roberts, A.P. & Barker, A.J., 2002. A late diagenetic (synfolding) magnetization carried by pyrrhotite: implications for palaeomagnetic studies from magnetic iron sulphide-bearing sediments, *Earth planet. Sci. Lett.,* **200,** 371–386.

Winkler, A., Florindo, F., Sagnotti, L. & Sarti, G., 1996. Inverse to normal magnetic fabric transition in an upper Miocene marly sequence from Tuscany, Italy, *Geophys. Res. Lett.,* **23,** 909–912.

Xu, W., van der Voo, R. & Peacor, D., 1998. Electron microscope and rock magnetic study of remagnetized Leadville carbonates, central Colorado, *Tectonophysics,* **296,** 333–362.